

# Last-layer committee machines for uncertainty estimations of benthic imagery

H. Martin Gillis<sup>a</sup>, Isaac Xu<sup>a</sup>, Benjamin Misiuk<sup>b,c</sup>, Craig J. Brown<sup>d</sup>, Thomas Trappenberg<sup>a,\*</sup>

<sup>a</sup>Faculty of Computer Science, Dalhousie University, Halifax, Nova Scotia, Canada

<sup>b</sup>Department of Earth Sciences, Memorial University of Newfoundland, St. John's, Newfoundland and Labrador, Canada

<sup>c</sup>Department of Geography, Memorial University of Newfoundland, St. John's, Newfoundland and Labrador, Canada

<sup>d</sup>Department of Oceanography, Dalhousie University, Halifax, Nova Scotia, Canada

## Abstract

Automating the annotation of benthic imagery (*i.e.*, images of the seafloor and its associated organisms, habitats, and geological features) is critical for monitoring rapidly changing ocean ecosystems. Deep learning approaches have succeeded in this purpose; however, consistent annotation remains challenging due to ambiguous seafloor images, potential inter-user annotation disagreements, and out-of-distribution samples. Marine scientists implementing deep learning models often obtain predictions based on one-hot representations trained using a cross-entropy loss objective with softmax normalization, resulting with a single set of model parameters. While efficient, this approach may lead to overconfident predictions for context-challenging datasets, raising reliability concerns that present risks for downstream tasks such as benthic habitat mapping and marine spatial planning. In this study, we investigated classification uncertainty as a tool to improve the labeling of benthic habitat imagery. We developed a framework for two challenging sub-datasets of the recently publicly available BenthicNet dataset using Bayesian neural networks, Monte Carlo dropout inference sampling, and a proposed single last-layer committee machine. This approach resulted with a  $> 95\%$  reduction of network parameters to obtain per-sample uncertainties while obtaining near-identical performance compared to computationally more expensive strategies such as Bayesian neural networks, Monte Carlo dropout, and deep ensembles. The method proposed in this research provides a strategy for obtaining prioritized lists of uncertain samples for human-in-the-loop interventions to identify ambiguous, mislabeled, out-of-distribution, and/or difficult images for enhancing existing annotation tools for benthic mapping and other applications.

**Keywords:** Benthic habitat mapping, human-in-the-loop, last-layer ensemble, Monte Carlo dropout, Bayesian neural network.

## 1. Introduction

Our oceans require better tools for management and oversight, monitoring seafloor (benthic) habitats, and assessing environmental impact indicators (Winther et al., 2020). Mapping benthic habitats has recently received much attention due to its importance in understanding changes in our oceans (Huang et al., 2011; Brown et al., 2011, 2012; Beijbom et al., 2016; Arosio et al., 2023; Misiuk and Brown, 2024). In part, this led to several large compilations of ocean floor imagery from research groups, government agencies, non-profit organizations, and other stakeholders from around the world (Brown et al., 2012; Katija et al., 2022; Humblot-Renaux et al., 2024; Misiuk et al., 2024; Lowe et al., 2025). For example, the recently publicly available BenthicNet (Lowe et al., 2025) consists of more than 11 million images, including *ca.* 2.5 million annotations labeled according to the Collaborative and Automated Tools for Analysis of Marine Imagery (CATAMI) hierarchical classification scheme (Althaus et al., 2014, 2015). It represents a diverse collection that can be used to develop and deploy deep learning networks to support automated mapping, understanding the

seafloor environment, and policy development for sustainable oceans and environmental management.

Most contemporary supervised methods train Convolutional Neural Networks (CNNs) such as Residual Networks (ResNets) (He et al., 2016) or attention-based architecture such as Vision Transformers (ViTs) (Dosovitskiy et al., 2021) to predict a class label, given image data. A common classification model represents class membership using a one-hot representation, which can be optimized using the cross-entropy loss function. The softmax of the model outputs can be interpreted as the probability density function  $p(y | \mathbf{x}; \mathbf{w})$ , where  $y$  are the class predictions,  $\mathbf{x}$  are the image inputs for the network, and  $\mathbf{w}$  are the trainable parameters of the model. However, these networks are known to overestimate the confidence of their output predictions (Holm et al., 2023; Szegedy et al., 2015; Wei et al., 2022). In these cases, the normalized outputs of the model (*i.e.*, softmax) often result with preferred predictions, even in cases where the predictions are incorrect. This is particularly problematic for marine image data, which are notoriously difficult to annotate (Ovadia et al., 2019; Humblot-Renaux et al., 2024; Xu et al., 2024). Oceanographers are therefore interested in tools that can provide them with per-sample reliability scores so that they can identify images that can be inspected manually.

Uncertainty in predictions can be derived from different

\*Corresponding author.

E-mail address: [tt@cs.dal.ca](mailto:tt@cs.dal.ca) (Thomas Trappenberg).

sources (Abdar et al., 2021; Gawlikowski et al., 2023; Hüllermeier and Waegeman, 2021). For example, data (aleatoric) uncertainty is inherent to the data itself, such as measurement noise and/or mislabeling or annotation errors. Collecting additional data would not reduce the uncertainty. Another source is model (epistemic) uncertainty, which reflects the lack of knowledge (or data) for the model to describe. Thus, in the limit of training with infinite data, model uncertainty can be reduced. An example would be out-of-distribution images (Ovadia et al., 2019), where a model attempts to make predictions for which it lacks representations (e.g., images from different geographic locations). In this case, these images can also reduce performance and potential applications of deep learning networks for benthic mapping. We therefore seek a strategy to identify uncertain or difficult images that can either be removed because of poor quality and/or submitted for subject matter expert interventions. In more general terms, we are interested in not only the most likely prediction for a single input image, but also how confident the network is for a difficult prediction. In addition, we require a scalable approach for large benthic image datasets that are constantly evolving over time to provide reliable information for changing environmental conditions (Li and Wang, 2023). Given the recent advances for uncertainty estimations for deep neural networks (Abdar et al., 2021; Gawlikowski et al., 2023), we seek an efficient strategy to identify a prioritized list of uncertain samples for Subject Matter Expert (SME) re-evaluations. In this work, *we propose to use classification as an approach to identify uncertain samples by comparing common uncertainty evaluators such as Bayesian Model Averaging (BMA) and Monte Carlo Dropout (MCD) to a proposed single Last-Layer Committee Machine (LLCM).*

Our main motivation for using a single last-layer committee machine is to provide a modular and compute-efficient approach for rapid access to obtain per-sample uncertainties. This approach goes beyond standard metrics (e.g., accuracy) that enables a human-in-the-loop strategy for re-evaluating difficult samples (Liu et al., 2022). An LLCM can provide this with a single forward pass of inputs during inference. Specifically, we use only one fully-connected layer for each member of the committee machine. This dramatically reduces the number of network parameters used to generate per-sample uncertainties. This is in contrast to BMA and MCD approaches where the entire network is sampled multiple times (e.g., 100+) to obtain per-sample uncertainties. For example, when using a feature extracting network with 100K parameters and a classification network with 1K parameters, sampling this network 100× (e.g., MCD) requires evaluating *ca.* 10M parameters to obtain per-sample uncertainties. When using an LLCM with the same feature extracting network and a classification network defined with 100 last-layer committee members with 1K parameters each, the resulting network involves a total of 200K parameters (sampled only once). This represents a *ca.* 98% reduction of network parameters to obtain per-sample uncertainties.

The gradients of each committee member of an LLCM module are independently backpropagated (i.e., no logit averaging) without the need for sophisticated loss functions or network configurations. The requisite committee member diversity was

obtained by randomly initializing network weights without applying additional techniques during training to promote diversity. Random initialization and the stochastic nature of training were sufficient to provide a set of uncertain samples. This was further investigated by comparing the coefficients of variation of learned committee members’ network weights and singular values from singular value decompositions of network weights during and after training.

To generate prioritized lists of uncertain samples for different uncertainty evaluators, we applied increasing threshold values of confidence scores (i.e., maximum softmax probabilities). The accuracies of the resulting subset of predictions (i.e., removal of difficult image predictions) were then plotted with respect to the fraction of samples remaining and confusion matrices were used to extract the corresponding remaining fractions of correct and incorrect model predictions to compute an efficiency metric. This is an unbiased approach for removal of uncertain samples as it evaluates network predictions that were both correct and incorrect. These uncertainty metric plots provided additional insights into the overall effectiveness of selecting different threshold values and comparing uncertainty evaluators.

The main contributions of our work can be summarized as the following:

- We propose a single LLCM classifier providing an efficient and scalable approach to obtain per-sample uncertainties.
- We present uncertainty metric plots as a data analysis tool to provide information on network performance and selectivity based on selected threshold values.
- Lastly, based on our analyses of network weights, we provide support that random initializations of committee members is sufficient to obtain epistemic (model) uncertainty.

To present our contributions, apart from this section, this paper is organized in the following sections: 1) Related work. In this section we discuss the challenges of annotating benthic images and techniques used to evaluate uncertainty estimates. 2) Methods. This section presents the framework for uncertainty evaluators, definition of the LLCM, loss calculation, and per-sample uncertainty estimations. In addition, this section includes descriptions for datasets, network configurations and calibration, and evaluation metrics. 3) Experiments. Here, we present our results to confirm network diversity of LLCM members and a comparison of uncertainty evaluators for a benchmark study and benthic images. 4) Conclusions. We provide concluding comments for the LLCM framework for improving uncertainty estimations for benthic imagery and other domain areas.

## 2. Related work

Despite having access to high-quality and large-scale benthic images, these datasets can still contain difficult images for networks and human annotators (Brown et al., 2012; Misiuk and

Brown, 2024; Humblot-Renaux et al., 2024). This can drastically impede the development of robust automated tools for benthic habitat mapping and decision-support for ocean management. Combined with changing benthic habitats, network performance is continuously challenged with exposure to unseen images that can limit practical applications in real-world monitoring. Many studies for benthic habitat mapping using neural networks focus on developing large datasets and applying transfer learning techniques to boost overall performance.

During their study of coral reefs in the Gulf of Eilat (Aqaba), Raphael et al. (2020) acquired *ca.* 5000K images with 11 different coral species. The authors reported classification accuracies of 80% when using pre-trained ResNet-50 networks and 90% when using VGG-16 (Simonyan and Zisserman, 2014) networks. Yasir et al. (2021) also investigated the classification of coral reefs. In this case, the authors incorporated two image enhancement strategies in addition to a pre-trained DenseNet-169 network to obtain an accuracy of 87% for 9 classes. Using a dataset of 70000 benthic images consisting of coral and substrate images (*i.e.*, sand/mud, pebbles/gravel+cobbles, and rocks), Jackett et al. (2023) obtained an accuracy of 98% for a pre-trained ResNet-50 network. The authors performed additional data pre-processing and applied several random augmentations such as, rotation, erasing, perspective, affine, and equalize during training. As part of the BenthicNet dataset, the authors also provided their results for the Substrate (depth 2) and German Bank 2010 sub-datasets (Lowe et al., 2025). Using a pre-trained ResNet-50 network trained using a supervised (cross-entropy) or self-supervised (Barlow Twins) objective function, the authors obtained 88% and 77% accuracy for the Substrate (depth 2) and German Bank 2010 sub-datasets, respectively.

An important component for a robust annotating tool for benthic mapping is addressing potential distribution shifts. This can result from a distal effect, where images from a geographic region are not represented in the current weights of the network. Humblot-Renaux et al. (2024) (Denmark) recognized that the BenthicNet dataset was lacking images for their geographic region. Subsequently, Humblot-Renaux et al. collected benthic images from video clips and created the JAMBO dataset (3290 images). This dataset was then trained using several pre-trained networks to obtain cross-validation F1-scores of 92%. The authors also evaluated the inter-rater reliability for human annotations of the testing images ( $N = 6$ ), resulting with an uncertainty evaluation of 84% for differentiating sand vs. stone benthic images. In addition to the distal effect on distribution shifts, there exists a temporal effect where geographic regions change over time and remains an open problem (Humblot-Renaux et al., 2024) Identifying a prioritized list of difficult or uncertain samples for human-in-the-loop interventions may offer an efficient strategy to address these distribution shifts.

Uncertainty estimates are often obtained using BMA of Bayesian Neural Networks (BNN) (Neal, 1995; Arbel et al., 2023; Jospin et al., 2020), Bayesian approximating methods such as, Monte Carlo Dropout (MCD) inference sampling (Gal and Ghahramani, 2015; Gal et al., 2017; Xie et al., 2021), and

deep ensembles (Lakshminarayanan et al., 2017; Pearce et al., 2018; Egele et al., 2021). However, these approaches have significant computational requirements as multiple networks are trained and evaluated (multiple times) during inference. To address this issue, strategies such as SnapShot ensembles (Huang et al., 2017) and BatchEnsembles (Wen et al., 2020) were developed. Another popular area of research to reduce computational requirements are “last-head” versions of deep ensemble networks whereby representation learning is decoupled from uncertainty estimations (Lee et al., 2015; Valdenegro-Toro, 2023; Harrison et al., 2024; Steger et al., 2024).

Lee et al. (2015) introduced a TreeNet deep ensemble architecture as a last-head ensemble where each head consists of one or more convolutional blocks (*i.e.*, a convolution and pooling layer) with the last block containing a fully-connected and softmax prediction layer. The authors highlighted that random initialization of shared network parameters can outperform full ensembles, dramatically reducing the computational requirements. The authors proposed an ensemble aware loss function that seeks to promote network diversity *via* multiple choice learning. In contrast to the proposed LLCM, a single fully-connected layer is used for each committee member (*i.e.*, no convolution or pooling layers), where the module consists of 100 committee members as opposed to the 5 heads reported by Lee et al.. In our case, network diversity was derived from the random initialization of network parameters using the cross-entropy loss function for training.

Valdenegro-Toro (2023) followed-up on the Lee et al. study, proposing deep sub-ensembles as an approach to obtain fast estimations of uncertainties. The authors used a similar last-head strategy, defining a single trunk network for representation learning and multiple task networks for uncertainty estimations. The main difference of deep sub-ensembles is the trunk network is initially trained and then the weights are fixed before training with multiple task networks. Compared to the LLCM, deep sub-ensembles approach uses multiple network layers for each head and involves additional pre-training steps to obtain uncertainties. The authors report using up to 15 heads for their deep sub-ensembles, compared to the 100 committee machine members we used for this study, which is made possible by extending a single LLCM. LLCMs provide an end-to-end approach where uncertainty estimations are obtained in a single forward-pass of inputs.

Perhaps closest to our work in terms of last-layer vs. last-head strategies are two recent works of Harrison et al. (Harrison et al., 2024) and Steger et al. (Steger et al., 2024) in 2024. Harrison et al. proposed using a Variational Bayesian Last-Layer Network (VBLL), while Steger et al. introduced Particle-Optimization Variational Inference (POVI) for a last-layer network trained in function space. These techniques can be used to separate representation learning and uncertainty estimations, which would be applicable for pre-trained networks.

While these last-head approaches (*i.e.*, TreeNets and deep sub-ensembles) reduced computational requirements, they come with additional steps to promote network diversity and/or specialized training procedures. Whereas the last-layer Bayesian techniques (*i.e.*, VBLL, and POVI) are often difficult

to configure for large datasets, such as BenthicNet. The LLCM further simplifies these techniques by using a single last-layer module and random initialization of network weights. In this study, we compare the LLCM to MCD inference sampling and fully Bayesian networks for a benchmark experiment and last-layer Bayesian networks for the more challenging benthic imagery. We show that LLCMs provide comparable uncertainty estimations and obtain results in an efficient single forward-pass of inputs.

### 3. Methods

In this section, we describe uncertainty evaluators and our proposed LLCM. We provide experimental details relating to data collection and processing, network configurations, hyperparameters, and network calibrations. We then demonstrate this approach to identify uncertain samples using different uncertainty evaluators: BMA, MCD, and our proposed LLCMs. Using the challenging benthic images from the publicly available high-resolution BenthicNet dataset (Misiuk et al., 2024; Lowe et al., 2025), we were able to obtain uncertain samples for subject matter expert interventions.

#### 3.1. Uncertainty evaluators

An approach for quantifying model uncertainty are Bayesian (or equivalent approximation) models, where a distribution of models are derived from learned parameters. Therefore, in terms of Bayesian analysis, we assess not only one model, but all possible models given the training data  $\mathcal{D}$ . The posterior predictive distribution (Eq. 1) is computed by marginalizing out all possible parameters (*i.e.*, by integration).

$$p(y|\mathbf{x}, \mathcal{D}) = \int_{\mathbf{w}} p(y|\mathbf{x}; \mathbf{w}) p(\mathbf{w}) d\mathbf{w} \quad (1)$$

$$\approx \frac{1}{M} \sum_{m=1}^M p(y|\mathbf{x}; \mathbf{w}^m) \quad (2)$$

However, for most cases this approach is computationally intractable. To address this challenge, Bayesian approximation methods were developed such as Monte Carlo dropout inference sampling (Gal and Ghahramani, 2015) and deep ensembles (Lakshminarayanan et al., 2017), including the last-layer strategies discussed in Section 2. This is achieved by averaging network predictions (Eq. 2) where  $M$  represents the number of models and individual probability distributions are calculated from output logits using network weights  $\mathbf{w}^m$  and the softmax function.

*Last-layer committee machines.* A last-layer committee machine (or ensemble) is a form of an ensemble classifier used to boost model performance and resulting predictions by averaging multiple models, often used with classification and regression trees such as random forests. Rather than using the full network as an ensemble, we used a list of  $M$  linear layers as a modular component for the network architecture (Eq. 3).

Table 1: Symbols and notations.

Symbol	Description
$\mathcal{D}$	Dataset
$\mathbf{x}$	Input data
$y$	Output data
$\mathbf{w}$	Weights of the model
$\mathbf{w}^m$	Weights of the $m^{\text{th}}$ model in the ensemble
$p(y \mathbf{x}, \mathcal{D})$	Posterior predictive distribution
$\mathbf{x} \rightarrow f(\mathbf{x}; \mathbf{w}^f)$	Feature extraction function
$g^m(f; \mathbf{w}^{g^m})$	Uncertainty estimation function for the $m^{\text{th}}$ committee member
$\mathcal{L}$	Total loss
$\ell^m(y, g^m(f; \mathbf{w}^{g^m}))$	Loss for the $m^{\text{th}}$ committee member
$M$	Number of models or committee members
$\mathbf{w}^{g^m}$	Weights of the $m^{\text{th}}$ model for uncertainty estimation
$\mu$	Mean value for image normalization ( <i>e.g.</i> , for BenthicNet)
$\sigma$	Standard deviation for image normalization ( <i>e.g.</i> , for BenthicNet)
$N$	Number of samples
$p(y_n \mathbf{x}_n)$	Predicted probability for the $n^{\text{th}}$ sample
$\mathbb{I}(y_n = 1)$	Indicator function for the true label $y_n = 1$
$B_m$	Set of samples in the $m^{\text{th}}$ bin (for ECE calculation)
$A_k(B_m)$	Accuracy for class $k$ in the $m^{\text{th}}$ bin (for ECE calculation)
$C_k(B_m)$	Mean predicted confidence for class $k$ in the $m^{\text{th}}$ bin (for ECE calculation)
$K$	Number of classes
$ B_m $	Number of samples in the $m^{\text{th}}$ bin
CV	Coefficient of variation calculated as $\sigma/\mu$
$\sigma_{\text{CV}_M}$	Standard deviation of the CV across $M$ committee members
$Z_m$	Output weight matrix for committee member $m$ of dimension $m \times n$
$U_m$	Left singular vectors of dimension $m \times m$
$\Sigma_m$	Singular values matrix of dimension $m \times n$
$V_m^T$	Right singular vectors of dimension $n \times n$
$\text{SV}_m^i$	The $i^{\text{th}}$ singular value from the singular value matrix $\Sigma_m$ of the $m^{\text{th}}$ committee member
$\text{CV}_{\text{SV}_M^i}$	Coefficient of variation of the respective $\text{SV}_m^i$ across $M$ committee members
$\text{CV}_{\ \text{SV}\ _F}$	Coefficient of variation of the Frobenius norm of singular values across $M$ committee members

$$\mathbf{x} \rightarrow f(\mathbf{x}; \mathbf{w}^f) \xrightarrow{m} g^m(f; \mathbf{w}^{g^m}) \rightarrow p(y|\mathbf{x}; \mathbf{w}^{g^m}) \approx p(y|\mathbf{x}, \mathcal{D}) \quad (3)$$

This approach separates the network into a two distinct networks for representation learning  $f(\mathbf{x}; \mathbf{w}^f)$  of inputs  $\mathbf{x}$  and uncertainty estimation  $g^m(f; \mathbf{w}^{g^m})$ . In this case, representations of



input images  $\mathbf{x}$  are created (e.g., ResNet-50) and passed to multiple uncertainty networks  $g^m$ , where each uncertainty network (i.e., committee member) is randomly initialized with different sets weights. Rather than backpropagating mean logit outputs of committee members, gradients of the computed loss of each committee member  $\ell^m(y, g^m(f; \mathbf{w}^m))$  are independently backpropagated as loss  $\mathcal{L}$  (Eq. 4).

$$\mathcal{L} = \ell^1(y, g^1(f; \mathbf{w}^1)) + \dots + \ell^m(y, g^m(f; \mathbf{w}^m)) \quad (4)$$

For every forward-pass during training, each committee member  $m$  receives identical feature representations  $f(\mathbf{x}; \mathbf{w}^f)$ ; therefore, network diversity or loss exploration during backpropagation is dependent on the initialization of each member. If committee machine members are identically initialized, they will all have the same weights during and after training, where the loss landscape exploration will be identical for each member. However, if they are non-identically initialized, the loss landscape exploration will be unique for a given committee member. During inference, individual probability distributions  $p(y|\mathbf{x}; \mathbf{w}^m)$  are calculated from output logits from using network weights  $\mathbf{w}^m$  and the softmax function, which are then averaged over  $M$  committee members to obtain the posterior predictive distribution as per-sample uncertainties (Eq. 5).

$$p(y|\mathbf{x}, \mathcal{D}) \approx \frac{1}{M} \sum_{m=1}^M \frac{e^{g^m(f; \mathbf{w}^m)}}{\sum e^{g^m(f; \mathbf{w}^m)}} \quad (5)$$

These simple modifications results with a network architecture that can provide epistemic uncertainty for both the dataset and single samples at inference. It drastically reduces computational and memory intensive requirements and can be parallelized and/or scaled to multiple devices. In addition, LLCMs can be used with different feature extracting networks to easily separate feature representations from uncertainty estimations.

### 3.2. Data collection and processing

**MNIST.** The MNIST dataset was used for the benchmark study which was obtained from the PyTorch dataset library and used without any further processing. Training, validation, and testing datasets were created using 50000 samples for training and 10000 samples each for validation and testing datasets. Class weights were also computed for the training dataset.

**German Bank 2010.** The German Bank dataset consists of 3181 samples of five classes that describe the seafloor environment such as: silt/mud, silt with bedforms, reef, glacial till, and sand with bedforms. Training and testing datasets were created by using the provided partition labels available in the annotation file (Misiuk et al., 2024). This resulted with a training dataset consisting of 2681 samples of silt/mud (23%), silt with bedforms (7%), reef (20%), glacial till (27%), and sand with bedforms (23%). The testing dataset contains 500 samples of silt/mud (42%), silt with bedforms (6%), reef (20%), glacial till (7%), and sand with bedforms (25%). The validation dataset was created by performing an 80:20 split of the training dataset, with label partitioning to ensure a balanced representation of

class labels in both datasets. Class weights were then computed for the resulting training dataset. Images were resized to  $224 \times 224$  and normalized using the BenthicNet corresponding means ( $\mu = [0.359, 0.413, 0.386]$ ) and standard deviations ( $\sigma = [0.219, 0.215, 0.209]$ ).

**Substrate (depth 2).** The Substrate dataset consists of 57149 samples of five classes that describe the seafloor environment such as: boulders, cobbles, rocks, pebbles/gravel, and sand/mud. As was done for the German Bank dataset, the training and testing datasets were created using the provided partition labels available in the annotation file (Misiuk et al., 2024). In this case, the training dataset consists of 43430 samples of boulders (5%), cobbles (2%), rocks (13%), pebbles/gravel (6%), and sand/mud (74%). Whereas, the testing dataset contains 13719 samples of boulders (3%), cobbles (2%), rocks (17%), pebbles/gravel (5%), and sand/mud (73%). The validation dataset was created as described above. Class weights were computed for the training dataset and all images were resized and normalized as described above.

### 3.3. Network configurations, hyperparameters, and calibrations

**Bayesian neural networks.** For the MNIST dataset a Bayesian neural network (BNN) was created by converting a baseline CNN using utilities available from the Pyro framework (Bingham et al., 2019) with an initialized mean and standard deviation of 0 and 1, respectively. The baseline network consisted of a feature extraction module with two blocks of convolutions, ReLU activations, and a maxpooling layer. Both blocks used convolution with 128 output channels, a kernel size of 5, and a maxpooling layer with a kernel and stride size of 2. The second block was subsequently flattened before being passed to a linear layer (2048 input and 2048 output channels) and ReLU activation. A classifier was added which consisted of a linear layer (2048 input and 10 output channels). Training (i.e., stochastic variational inference) was performed over 25 epochs using default values of the Pyro ClippedAdam optimizer with a learning rate of  $1.0 \times 10^{-3}$  and the evidence lower bound (ELBO) loss objective function using the Categorical distribution represented by logits and target labels (Table 2). In the case of the BenthicNet datasets, last-layer Bayesian networks (Harrison et al., 2024) were created using a BenthicNet pre-trained ResNet-50 model (Xu et al., 2024). The fully-connected component was modified with a linear layer (2048 input and output channels, respectively) followed by batch normalization, and ReLU activation. A classifier was added which consisted of a linear layer (2048 input and 5 output channels) which was converted to a Bayesian layer using utilities from the Pyro framework. The German Bank 2010 dataset (batch size 128) was trained over 200 epochs using the Pyro ClippedAdam optimizer with a learning rate of  $1.75 \times 10^{-3}$  and default values, except for gradient clip normalization which was set to 1.0. The Substrate (depth 2) dataset (batch size 128) was trained over 15 epochs with a learning rate of  $1.0 \times 10^{-3}$  with all other settings set to their default values (Table 2).

Table 2: Network configurations and hyperparameters.

Dataset	Network <sup>1-6</sup>	Epochs	Optimizer	Learning Rate	Scheduler	Criterion	Weight Decay	Label Smoothing
MNIST	BNN	25	ClippedAdam	$1.0 \times 10^{-3}$	None	ELBO	None	None
	CNN	100	Adam	$1.0 \times 10^{-5}$	None	CrossEntropyLoss	0.0	0.0 or 0.1
	LLCM	100	Adam	$1.0 \times 10^{-5}$	None	CrossEntropyLoss	0.0	0.0 or 0.1
German Bank	ResNet-BNN	200	ClippedAdam (1.0)	$1.75 \times 10^{-3}$	None	ELBO	None	None
	ResNet-CNN	50	Adam	$3.0 \times 10^{-6}$	OneCycleLR	CrossEntropyLoss	$1.0 \times 10^{-5}$	0.0 or 0.1
	ResNet-LLCM	25	Adam	$3.0 \times 10^{-6}$	OneCycleLR	CrossEntropyLoss	$1.0 \times 10^{-5}$	0.0 or 0.1
Substrate	ResNet-BNN	15	ClippedAdam	$1.0 \times 10^{-3}$	None	ELBO	None	None
	ResNet-CNN	25	Adam	$1.0 \times 10^{-5}$	OneCycleLR	CrossEntropyLoss	$1.0 \times 10^{-3}$	0.0 or 0.1
	ResNet-LLCM	25	Adam	$3.0 \times 10^{-6}$	OneCycleLR	CrossEntropyLoss	$1.0 \times 10^{-5}$	0.0 or 0.1

<sup>1</sup> BNN: [Conv(128, 5×5)–ReLU–MaxPool(2×2)]<sub>2</sub>–FC(2048)–FC(10) <sup>2</sup> CNN: [Conv(128, 5×5)–ReLU–MaxPool(2×2)–Dropout( $p$ )]<sub>2</sub>–FC(2048)–FC(10) <sup>3</sup> LLCM: [Conv(128, 5×5)–ReLU–MaxPool(2×2)–Dropout( $p$ )]<sub>2</sub>–FC(2048)–[FC(10)]<sub>100</sub> <sup>4</sup> ResNet-BNN: ResNet(BottleNecks)–FC(2048)–BatchNorm–ReLU–Bayesian–FC(5) <sup>5</sup> ResNet-CNN: ResNet(BottleNecks)–FC(2048)–BatchNorm–ReLU–Dropout( $p$ )–FC(5) <sup>6</sup> ResNet-LLCM: ResNet(BottleNecks)–FC(2048)–BatchNorm–ReLU–Dropout( $p$ )–[FC(5)]<sub>100</sub>

*Convolutional neural networks.* Using the above baseline CNN for the MNIST dataset, a dropout layer was added after each pooling layer with a dropout rate of 0.1. The dataset (batch size 128) was trained over 100 epochs using the Adam optimizer with a learning rate of  $1.0 \times 10^{-5}$  and the cross-entropy loss objective function with/without class weights and label smoothing (Szegedy et al., 2015) or with/without logit normalization (Wei et al., 2022) (Table 2). For the BenthicNet datasets, a BenthicNet pre-trained ResNet-50 model (Xu et al., 2024) was used with the addition of a dropout layer ( $p = 0.01$ ) after each ReLU activation of the BottleNeck block of the ResNet-50 architecture. The fully-connected component was modified with a linear layer (2048 input and output channels, respectively) followed by batch normalization, ReLU activation, and a dropout layer ( $p = 0.01$ ). A classifier was added which consisted of a linear layer (2048 input and 5 output channels). The German Bank 2010 dataset (batch size 128) was trained over 50 epochs using the Adam optimizer with a learning rate of  $3.0 \times 10^{-6}$ , weight decay of  $1.0 \times 10^{-5}$ , and the cross-entropy loss function with/without class weights, logit normalization, or label smoothing. The OneCycleLR scheduler (Smith and Topin, 2017; PyTorch, 2025b) was applied during training using an initial and final learning rate factor of 0.1, where the rate was increased over the first 10% of the total number of epochs. This was then repeated for the Substrate (depth 2) dataset over 25 epochs (Table 2).

*Last-layer committee machines.* For the MNIST dataset, a dropout layer was added after each pooling layer with a dropout rate of 0.1 and a list of committee members of size 100 as the classifier for the previously described baseline CNN. Training was done with a batch size of 128 over 100 epochs using the Adam optimizer with a learning rate of  $1.0 \times 10^{-5}$  and the cross-entropy loss objective function (for each  $M$  classifier), with/without class weights and label smoothing or with/without logit normalization. The total loss, mean probabilities, and corresponding standard deviations were computed as previously described (Section 3 and Table 2). For the ResNet-CNN models described above, the classifier was converted to a list of 100 classifiers with 5 output channels for the BenthicNet datasets. Training was performed over 25 epochs with a learning rate of

$3.0 \times 10^{-6}$ , weight decay of  $1.0 \times 10^{-5}$ , using the OneCycleLR scheduler as previously described. For both datasets, training was done using the cross-entropy loss objective function (for each  $M$  classifier), with/without class weights and label smoothing or with/without logit normalization. The total loss was then scaled by the number of committee members  $M$  (i.e., a scaling factor), before being backpropagated during training. This scaling factor can be considered an additional hyperparameter for training the network. During inference, mean probabilities and corresponding standard deviations were computed by averaging the normalized logit outputs from  $M$  committee members using the softmax function (Table 2).

*Network calibration.* Model calibration was performed by finding the optimal temperature (i.e., scaling of logits) that minimizes the cross-entropy loss on the validation dataset. This was achieved using a pre-trained model and Bayesian optimization with Gaussian Process (GP) regression (Louppe and Kumar, 2016). The optimization explored a temperature search space of 0.01–10.0, using a log-uniform prior which was configured to perform 50 evaluations of the objective function. For LLCM models, the temperature for each committee member was optimized separately. After finding the optimal temperature(s), the previously trained model was used to perform inference on the testing dataset, scaling the logits with the optimized calibrated temperature(s). Network calibration was then evaluated based on commonly used metrics such as: Negative Log-likelihood (NLL), Brier Score (BS), Expected Calibration Error (ECE) and Reliability Diagrams (Guo et al., 2017) as described in the next section.

*Network evaluation and metrics.* For applied applications, probabilities for predictions would ideally reflect observed accuracies, where predictions indicate how likely they are to be correct (Guo et al., 2017). For example, given network predictions with 80% probability, we expect the fraction correct would be 80% (perfectly calibrated). In general, Calibration Error (CE) can be measured as the difference of average confidence and accuracy. A negative calibration error indicate the model is under-confident and a positive calibration error indicate the model is over-confident. This is particularly important

for applications involving high-risk decision-making. To evaluate the quality of model calibrations, several common metrics are used such as NLL, BS, ECE, and reliability diagrams. The NLL is defined as the negative logarithm of the likelihood function, which represents the probability of the observed data given the model parameters (Eq. 6).

$$\text{NLL} = -\frac{1}{N} \sum_{n=1}^N \log p(y_n | \mathbf{x}_n) \quad (6)$$

The BS is calculated as the mean squared error of  $p(y|\mathbf{x})$  for the true predicted class and the corresponding one-hot encoded representations (Eq. 7),

$$\text{BS} = \frac{1}{N} \sum_{n=1}^N (p(y_n | \mathbf{x}_n) - \mathbb{I}(y_n = 1))^2 \quad (7)$$

where  $N$  is the total number of samples;  $p(y_n | \mathbf{x}_n)$  is the predicted probability for the positive class for the  $n^{\text{th}}$  sample; and  $\mathbb{I}(y_n = 1)$  is the indicator function, which is 1 if the true label  $y_n$  is 1 and 0 otherwise. The BS provides a metrics to score how well the dataset is calibrated with a value of 0 being perfectly calibrated. For a more discretized evaluation of the quality of model calibration, calibration errors can be calculated by partitioning confidence values into bins using a multiclass ECE as defined by (Eq. 8),

$$\text{ECE} = \sum_{m=1}^M \frac{|B_m|}{n} \sum_{k=1}^K |A_k(B_m) - C_k(B_m)| \quad (8)$$

where  $M$  is the number of bins;  $B_m$  is the set of samples whose predicted probabilities for the positive class are in the  $m^{\text{th}}$  bin;  $|B_m|$  is the number of samples in the  $m^{\text{th}}$  bin;  $n$  is the total number of samples;  $K$  is the number of classes;  $A_k(B_m)$  is the accuracy for class  $k$  in the  $m^{\text{th}}$  bin; and  $C_k(B_m)$  is the mean probability (confidence) for class  $k$  in the  $m^{\text{th}}$  bin.

Both the BS and ECE provides a scalar value that can be used to assess the quality of model calibrations; however, they do not distinguish whether a model is over- and/or under-confident. While the CE metric does provides an overall assessment (*i.e.*, under- vs. over-confident), it is insufficient for ranges of confidence values. In this case, a reliability diagram provides additional visual insights by comparing the mean predicted confidence in increasing discretized bins with the corresponding accuracy for a given bin. A well-calibrated model will produce a positive linear relationship, indicating that predicted probabilities align with correct model predictions. Deviations from this relationship provides insights whether the model is under- (values above the line) and/or over-confident (values below the line) in its predictions. We provide reliability diagrams with a histogram of confidence scores for each bin to assess the importance based on the total number of samples (normalized). Once an evaluation of model calibration is obtained, a calibration method can be applied as a post-processing step (if necessary). This is typically done with a validation dataset where a hyperparameter is adjusted to optimize model calibration. For classification tasks, temperature scaling (Gawlikowski et al.,

2023; Guo et al., 2017) during softmax normalization is an efficient method for model calibration. After training, a validation dataset is used for optimization (*e.g.*, Bayesian optimization) to find the ideal temperature, followed by a re-evaluation of model calibration. In addition to the above network evaluations, we also report accuracy for the each of the the different approaches for BNN, CNN, LLCM, and different hyperparameters (*e.g.*, label smoothing and logit normalization) for addressing over-confident network predictions.

## 4. Experiments

While developing the last-layer committee machines for benchtic imagery, we wanted to investigate network diversity across each committee member. In particular, we wanted to ensure sufficient diversity persists at the end of training that would support using random initialization of weights. We explored network diversity using statistical analyses of the coefficient of variations (CV) of committee members weights and corresponding singular value decompositions. As others have noted, random initialization is sufficient for deep ensemble last-head (Lee et al., 2015) and Bayesian last-layer (Steger et al., 2024) approaches. We provide additional empirical support for random initialization using LLCM, which avoids requiring specialized techniques to promote network diversity (Section 4.1).

For the subsequent sections, we then compare our LLCM with two commonly used approaches to obtain uncertainty estimations: 1) Bayesian model averaging of BNNs; and 2) Monte Carlo dropout inference sampling of CNNs. It is important to note that our focus here is not necessarily to identity a *better performing model*; rather, to find an *equivalent performing model* with reduced compute requirements and complexities. We provide a benchmark study and the results for the more challenging German Bank 2010 and Substrate (depth 2) datasets.

### 4.1. Network diversity

**Committee member weights.** Our initial approach to investigate network diversity used a trained LLCM-10 ( $p = 0.0$ ) network and the MNIST dataset. After training, each committee member classifier weights were flattened and the coefficient of variations were computed. Committee members with similar CV values would equate to being similar. In this case, we expect the standard deviations of CV across committee members to be zero. To confirm this hypothesis, we prepared a network where all committee members weights were initialized with ones. Table 3 shows the results of using different hyperparameters during training, such as class weighting, logit normalization, and label smoothing. Although not required for this analysis, calibration metrics are provided for comparison. The last entry of Table 3 shows the result where all committee machine members had weights initialized with ones. This resulted with a  $\sigma_{\text{CV}_M}$  of 0.0, which indicates that all members are identical.

The above approach provides support for network diversity and is a simple and convenient method; however, learned structural information may be lost as a result of exclusively using

**Table 3:** Network diversity ( $\sigma_{CV_M}$ ) and model performance of a LLCM-10 and the MNIST dataset.

Model <sup>1</sup>	Accuracy $\uparrow$	NLL $\downarrow$	BS $\downarrow$	ECE $\downarrow$	$\sigma_{CV_M}$
-/-/-	0.991	0.014	0.003	0.004	9.537
-/+/-	0.990	0.250	0.072	0.181	906.146
+/-/-	0.989	0.257	0.074	0.185	8372.234
+/-/+	0.991	0.014	0.003	0.003	9.414
+/-/+	0.992	0.141	0.026	0.115	25.502
-/-/+	0.992	0.141	0.026	0.115	23.713
-/-/- <sup>2</sup>	0.991	0.013	0.003	0.001	<b>0.0</b>

<sup>1</sup> Models defined based on training hyperparameters using class weights / logit normalization / label smoothing (amount of smoothing, 0.1). These hyperparameters are either applied (denoted by +) or omitted (denoted by -). <sup>2</sup> All committee machine members weights were initialized with ones.

learned classifier weights values. In addition, a large increase in network diversity ( $\sigma_{CV_M}$ ) was observed when using logit normalization. While this is expected given that logit normalization operates by factoring the magnitude of weight vectors, it does highlight potential numerical stability issues when calculating CV values (*i.e.*,  $CV = \frac{\sigma}{\mu}$ ). For this reason, we next explored singular value decomposition analyses (*vide infra*) of network weights for each committee member during and after training.

**Committee member singular value decompositions.** In this case, we extracted Singular Values (SV) from classifiers weights using Singular Value Decomposition (SVD) and compare weights during and after training. SVD is a linear algebra technique used to decompose a matrix into three corresponding matrices involving a rotation, re-scaling, and then another rotation and is defined as  $\mathbf{Z}_m = \mathbf{U}_m \mathbf{\Sigma}_m \mathbf{V}_m^T$ , where  $\mathbf{Z}_m$  is an output matrix for committee member  $m$  of dimension  $m \times n$ ; left singular vectors  $\mathbf{U}_m \in \mathbb{R}^{m \times m}$ ; singular values  $\mathbf{\Sigma}_m \in \mathbb{R}^{m \times n}$ ; and right singular vectors  $\mathbf{V}_m^T \in \mathbb{R}^{n \times n}$ . The diagonal of the  $\mathbf{\Sigma}_m$  represents the singular values (*i.e.*, unique values) of the  $m^{th}$  committee member of size  $\min(m, n)$ . A single scalar metric can be computed as the CV of the Frobenius norm of the SV for all committee members ( $CV_{\|SV\|_F}$ ). The Frobenius norm of the SV represents the overall magnitude (or energy). This metric measures the variation across all committee members, which would be 0 if members are identical. This strategy offers to maintain structural information and is less sensitive to outliers and numerical stability issues as compared to the above method. By comparing respective CV and Frobenius norm values of the singular values across each committee member, an evaluation of network diversity can be quantitatively measured.

We investigated identical and non-identical initialization strategies across committee members for a LLCM-10 ( $p = 0.0$ ) network and the MNIST dataset. In this case, there are a total of 10 singular values for each committee member reflecting the  $n = 10$  classes of the MNIST dataset. To gain additional insight during training, for each  $SV_m^i$  we computed the

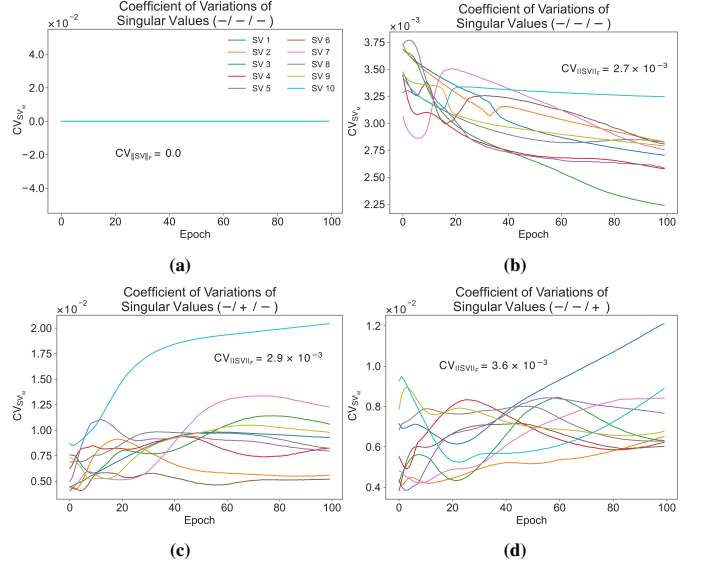


**Fig. 1:** Network diversity ( $CV_{SV_M^i}$  and  $CV_{\|SV\|_F}$ ) of a LLCM-10 and the MNIST dataset. Panel (a) shows the results of having identically initialized members, whereas panels (b–d) shows the results of random initialization using class weights / logit normalization / label smoothing (amount of smoothing, 0.1). These hyperparameters are either applied (denoted by +) or omitted (denoted by -).

CV across all committee members  $m$  ( $CV_{SV_M^i}$ ). We then plotted  $CV_{SV_M^i}$  to observe the variation of the  $SV_M^i$  during training to confirm if committee members are converging (Fig. 1). When identically initializing all committee members using the same random seed, we observed no variation of  $CV_{SV_M^i}$  or  $CV_{\|SV\|_F}$  (Fig. 1a). However, when committee members are randomly initialized and trained using different hyperparameters such as cross-entropy (Fig. 1b) with logit normalization (Fig. 1c) or label smoothing (Fig. 1d), after training we observe  $CV_{\|SV\|_F}$  is non-zero and  $CV_{SV_M^i}$  are non-identical. In contrast to the  $\sigma_{CV_M}$  analyses of committee members classifiers weights (Table 3) where a large range  $\sigma_{CV_M}$  values were obtained, the SVD analyses provided similar results when using different hyperparameters (*e.g.*, Fig. 1b–Fig. 1d:  $CV_{\|SV\|_F} 2.7 \times 10^{-3} - 3.6 \times 10^{-3}$ ).

#### 4.2. Uncertainty evaluators: A benchmark study

For our benchmark study, we used the well-known MNIST dataset and the network configurations as described above (Section 3). We first trained a baseline deterministic CNN model with a dropout rate of 0.1 using several combinations of techniques for addressing over-confidence (Table 4, CNN). When using logit normalization or label smoothing, we observed a noticeable decrease in model calibration as measured by NLL, BS, and ECE. All of which were resolved after re-calibration by applying a temperature-scaling (see Fig. 2). That is, values tended towards the values obtained without these techniques such as with/without class weighting using the cross-entropy loss function. This suggests that the networks were already well-calibrated and these steps may not have been required. However, it would be quite prudent to first measure the amount of network calibration before applying these techniques. We



**Table 4:** Model performances using ensemble and non-ensemble models and the MNIST dataset.

Model <sup>1,2</sup>	Accuracy $\uparrow$	NLL $\downarrow$	BS $\downarrow$	ECE $\downarrow$
<b>Non-ensemble: CNN (<math>p = 0.1</math>)</b>				
-/-/-	0.992	0.011 (0.007)	0.003 (0.002)	0.001 (0.003)
-/+/-	0.990	0.457 (0.015)	0.153 (0.004)	0.308 (0.004)
+/-/-	0.990	0.470 (0.016)	0.158 (0.004)	0.316 (0.004)
+/-/+	0.991	0.011 (0.007)	0.003 (0.002)	0.001 (0.003)
+/-/+	0.993	0.141 (0.008)	0.025 (0.002)	0.117 (0.001)
-/-/+	0.991	0.258 (0.009)	0.059 (0.002)	0.208 (0.003)
<b>Ensemble: BMA-100</b>				
BNN	0.967	0.164	0.041	0.101
<b>Ensemble: MCD-100 (CNN; <math>p = 0.1</math>)</b>				
-/-/-	0.991	0.016 (0.011)	0.004 (0.003)	0.005 (0.001)
-/+/-	0.989	0.419 (0.015)	0.137 (0.004)	0.285 (0.002)
+/-/-	0.989	0.431 (0.016)	0.141 (0.004)	0.293 (0.002)
+/-/+	0.991	0.015 (0.011)	0.004 (0.003)	0.004 (0.002)
+/-/+	0.993	0.140 (0.010)	0.025 (0.002)	0.115 (0.001)
-/-/+	0.992	0.365 (0.055)	0.099 (0.010)	0.287 (0.039)
<b>Ensemble: LLCM-100 (LLCM; <math>M = 100</math>; <math>p = 0.1</math>)</b>				
-/-/-	0.992	0.011 (0.009)	0.003 (0.002)	0.002 (0.002)
-/+/-	0.991	0.558 (0.015)	0.196 (0.004)	0.362 (0.005)
+/-/-	0.991	0.539 (0.015)	0.188 (0.004)	0.352 (0.005)
+/-/+	0.993	0.012 (0.009)	0.003 (0.002)	0.003 (0.002)
+/-/+	0.993	0.141 (0.008)	0.024 (0.002)	0.117 (0.001)
-/-/+	0.994	0.139 (0.008)	0.024 (0.002)	0.116 (0.001)

<sup>1</sup> BMA: 100 models; MCD: 100 inference samplings; and LLCM: 100 committee members. <sup>2</sup> Models defined based on training hyperparameters using class weights / logit normalization / label smoothing (amount of smoothing, 0.1). These hyperparameters are either applied (denoted by +) or omitted (denoted by -). Values in parentheses are for calibrated models using calculated temperature(s) as previously described.

applied these technique here to gain a overall impression on the effect of results to make generalizations.

We now compare the different uncertainty evaluators (BMA, MCD, LLCM) for the MNIST dataset. We converted the CNN network to a BNN ( $p = 0.0$ ) using the tools available from the Pyro framework. This BNN was then trained and BMA was performed by sampling 100 sets of weights from the learned distributions and evaluating the resulting ensemble (Table 4, BMA-100). While the overall performance was slightly less than the deterministic model (*ca.* 97% vs. 99%) this was not necessarily unexpected given that a different model, loss objective (*i.e.*, ELBO), and a dropout layer were used for the deterministic model. Monte Carlo dropout inference sampling was then performed using a trained CNN ( $p = 0.1$ ) with an inference dropout rate of 0.1, sampling 100 sets of weights, and evaluating the resulting ensemble (Table 4, MCD-100). As with the baseline CNN, we explored different techniques for addressing over-confidence, where the results were comparable to the CNN. Subsequently, we trained our LLCM model using 100 committee members with a dropout rate of 0.1 (Table 4, LLCM-100). In this case, sampling 100 sets of weights was not required as a single forward-pass returns per-sample uncertainties from the 100 committee members. For the BMA, MCD and LLCM networks, all corresponding models were comparable to

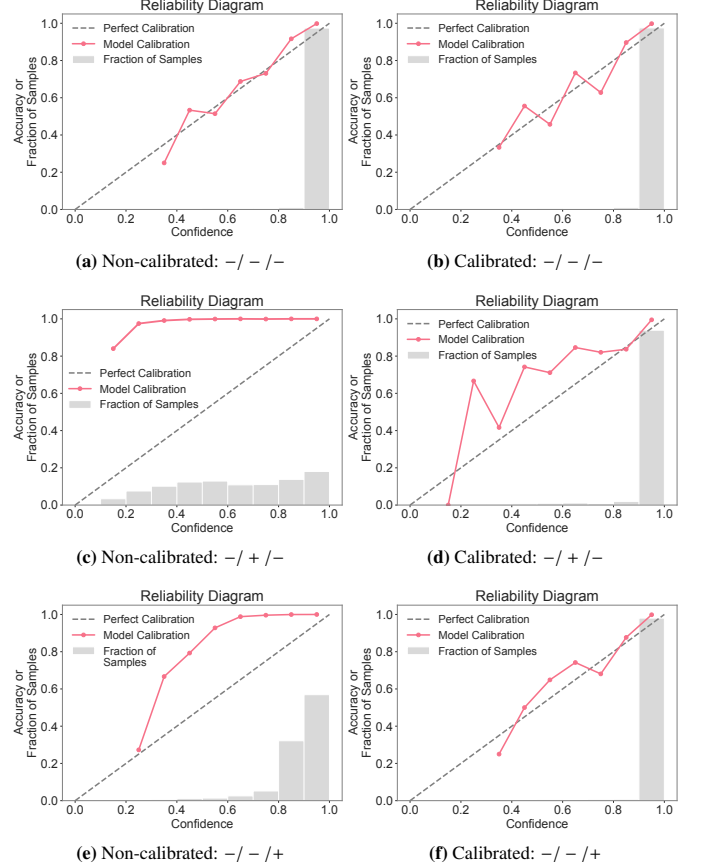


**Fig. 2:** Reliability diagrams for the MNIST dataset using an LLCM-100 network ( $p = 0.1$ ). Non-calibrated (left panels) and calibrated (right panels) using class weights / logit normalization / label smoothing (amount of smoothing, 0.1). These hyperparameters are either applied (denoted by +) or omitted (denoted by -).

the baseline CNN. However, the advantage of the LLCM compared to BMA or MCD is the reduced compute requirements without any performance loss.

For example, in this case, the CNN network used for MCD consists of *ca.* 400K network parameters which is sampled  $100\times$  (*i.e.*, 40M network parameters) to obtain per-sample uncertainties. Whereas, the LLCM network consists of *ca.* 2M network parameters which is evaluated only once. This represents a  $20\times$  reduction (95%) of network parameters to obtain per-sample uncertainties.

To compare the uncertainty estimations of BMA, MCD and LLCM networks, we plotted uncertain metric plots (Fig. 3). For illustration, we show the results using cross-entropy loss without logit normalization and label smoothing (*i.e.*, -/- / -). Both the MCD and LLCM provided similar results followed by BMA. Fig. 3b shows there is a preferential removal of incorrect model predictions (FP + FN) as opposed to correct model predictions (TP + TN) up to an optimal fraction. Recall that the fraction of remaining samples is calculated based on different threshold of confidence values. After this fraction, the differences of the removal rates are decreasing and do not offer additional benefits. In fact, performance is artificially enhances by the non-preferential removal of incorrect predictions.

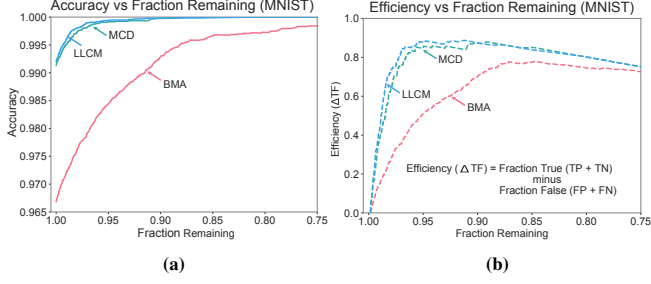


**Fig. 3:** Uncertain metric plots for the BMA-100, MCD-100 (–/–/–), and LLCM-100 (–/–/–) networks and the MNIST dataset using class weights / logit normalization / label smoothing (amount of smoothing, 0.1). These hyperparameters are either applied (denoted by +) or omitted (denoted by –). Each trace is created by applying increasing thresholds (step size 0.001) of confidence values and re-calculating metrics.

In summary, the benchmark study demonstrates that LLCMs can further simplify last-head strategies (see Section 2) by only using a single last-layer for uncertainty estimations. Both MCD and LLCM approaches resulted with similar performances (with slightly better performance than BMA); however, LLCMs dramatically reduces the computational requirements. Applying over-confident techniques such as logit normalization or label smoothing appeared to degrade model calibration, which can be corrected using temperature-scaling. Overall, this offers an efficient approach for Bayesian approximations and a strategy to identify uncertain model predictions for human-in-the-loop interventions.

#### 4.3. Uncertainty evaluators: Benthic imagery

**German Bank 2010 dataset.** The German Bank dataset consists of 5 classes of silt/mud, silt with bedforms, reef, glacial till, and sand with bedforms, and represents a difficult dataset for learning a model. The results of the dataset is summarized in Table 5. We initially trained a non-ensemble CNN (ResNet-CNN) with a dropout rate of 0.01 from a pre-trained model, using class weighting and/or different techniques for addressing over-confidence (Table 5, Non-ensemble). We obtained modest performance for accuracy and calibration metrics as observed from accuracies, NLL, BS, and ECE. In fact, model calibration decreased when using techniques for addressing over-confidence (e.g., logit normalization and label smoothing). A variational Bayesian last-layer network based on the pre-trained ResNet-CNN model was subsequently created and trained. After performing BMA with 100 samplings of weights, the performance was slightly less than the non-ensemble model (Table 5, BMA-100 vs. Non-ensemble).

In this case, the calibration metrics suggests that the model is poorly calibrated. We then performed Monte Carlo dropout inference sampling on the trained ResNet-CNN models (Table 5, Non-ensemble) by sampling 100 sets of weights during inference, which resulted with comparable metrics to the non-ensemble models (Table 5, MCD-100 vs. Non-ensemble). A similar trend for model calibrations were observed for the non-ensemble models. Lastly, we applied our LLCM by adding an LLCM-100 module to the ResNet-CNN network (Table 5, LLCM-100). After training and a single forward-pass of inputs

**Table 5:** Model performances using ensemble and non-ensemble models and the German Bank 2010 dataset.

Model <sup>1,2</sup>	Accuracy↑	NLL↓	BS↓	ECE↓
<b>Non-ensemble: ResNet-CNN (<math>p = 0.01</math>)</b>				
–/–/–	0.790	0.202 (0.200)	0.058 (0.057)	0.062 (0.060)
–/+/–	0.770	0.871 (0.201)	0.334 (0.060)	0.328 (0.082)
+/+/–	0.758	0.866 (0.198)	0.331 (0.059)	0.314 (0.101)
+/-/–	0.794	0.202 (0.188)	0.057 (0.053)	0.069 (0.075)
+/-/+	0.786	0.338 (0.189)	0.101 (0.052)	0.058 (0.077)
–/-/+	0.774	0.298 (0.196)	0.088 (0.055)	0.023 (0.070)
<b>Ensemble: BMA-100 (ResNet-BNN)</b>				
BNN	0.734	0.527	0.179	0.117
<b>Ensemble: MCD-100 (ResNet-CNN; <math>p = 0.01</math>)</b>				
–/–/–	0.794	0.225 (0.222)	0.065 (0.064)	0.059 (0.059)
–/+/–	0.772	0.917 (0.232)	0.355 (0.069)	0.351 (0.075)
+/+/–	0.762	0.910 (0.227)	0.352 (0.068)	0.339 (0.070)
+/-/–	0.788	0.226 (0.210)	0.065 (0.059)	0.037 (0.057)
+/-/+	0.784	0.370 (0.213)	0.112 (0.060)	0.068 (0.066)
–/-/+	0.788	0.330 (0.223)	0.099 (0.063)	0.044 (0.053)
<b>Ensemble: LLCM-100 (ResNet-LLCM; <math>M = 100</math>; <math>p = 0.01</math>)</b>				
–/–/–	0.786	0.151 (0.219)	0.040 (0.059)	0.099 (0.058)
–/+/–	0.774	0.636 (0.255)	0.227 (0.081)	0.207 (0.074)
+/+/–	0.758	0.651 (0.265)	0.233 (0.085)	0.200 (0.052)
+/-/–	0.788	0.145 (0.199)	0.037 (0.052)	0.099 (0.060)
+/-/+	0.788	0.301 (0.214)	0.083 (0.055)	0.047 (0.046)
–/-/+	0.782	0.252 (0.208)	0.067 (0.054)	0.054 (0.060)

<sup>1</sup> BMA: 100 models; MCD: 100 inference samplings; and LLCM: 100 committee members. <sup>2</sup> Models defined based on training hyperparameters using class weights / logit normalization / label smoothing (amount of smoothing, 0.1). These hyperparameters are either applied (denoted by +) or omitted (denoted by –). Values in parentheses are for calibrated models using calculated temperature(s) as previously described.

during inference, we obtained metrics that were comparable to both MCD-100, BMA-100, and non-ensembles models (with the exception of uncertainty metrics for BMA-100).

When using techniques for addressing over-confidence (Szegedy et al., 2015; Wei et al., 2022) with the non-ensemble networks and the MCD-100 and LLCM-100 ensemble networks (Table 5), we observed an appreciable decrease in model calibration. In Fig. 4 we plotted reliability diagrams for the LLCM-100 non-calibrated and calibrated models using cross-entropy loss with (–/ + /–) or without (–/–/–) logit normalization or label smoothing (–/–/+). The largest effect observed involved the use of logit normalization, where the model was under-confident with a near uniform distribution of confidence values. However, this was mostly restored after applying a re-calibration (Fig. 4d). This was also observed in our benchmark study for both logit normalization and label smoothing (Fig. 2).

We next used threshold confidence values to create lists of uncertain samples for the three uncertainty evaluators, BMA-100, MCD-100 (–/–/–), and LLCM-100 (–/–/–). To compare the different approaches, we varied threshold values of increasing increments of 0.001, calculated the corresponding accuracy and efficiency and created uncertain metric plots (Fig. 5). We opted to plot metrics vs. fraction remaining as

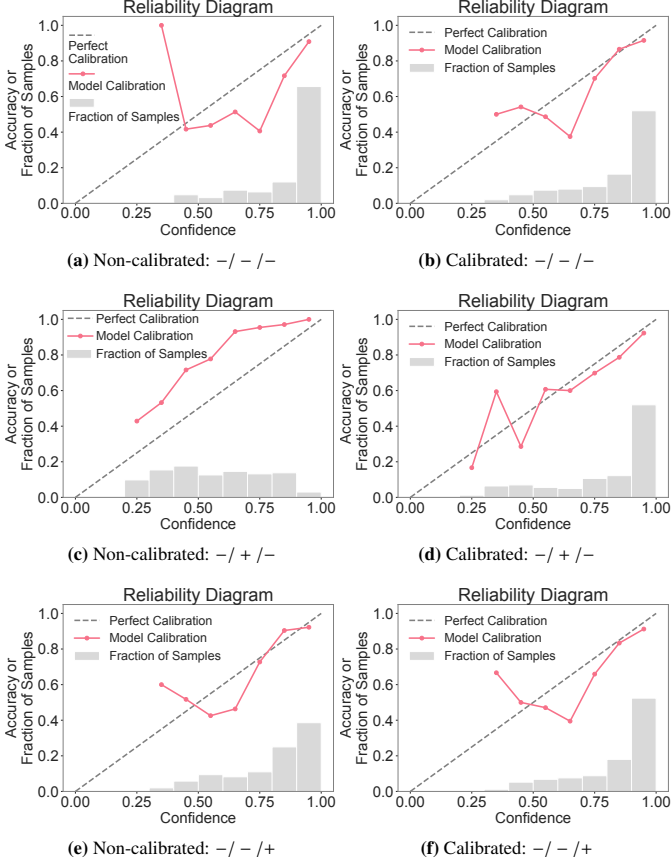


**Fig. 4:** Reliability diagrams for the German Bank 2010 dataset using a LLCM-100 network ( $p = 0.01$ ). Non-calibrated (left panels) and calibrated (right panels) using class weights / logit normalization / label smoothing (amount of smoothing, 0.1). These hyperparameters are either applied (denoted by +) or omitted (denoted by -).

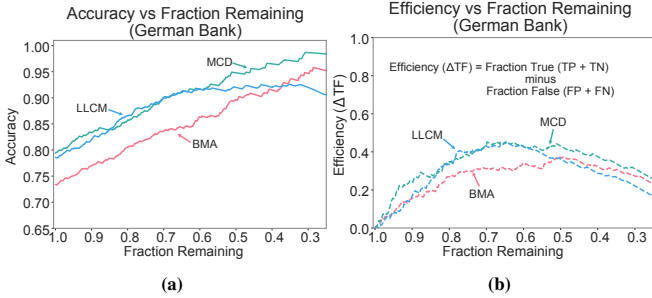


**Fig. 5:** Uncertain metric plots for the BMA-100, MCD-100 (-/- / -/), and LLCM-100 (-/- / -/) networks and the German Bank 2010 dataset using class weights / logit normalization / label smoothing (amount of smoothing, 0.1). These hyperparameters are either applied (denoted by +) or omitted (denoted by -). Each data point is created by applying increasing thresholds (step size 0.001) of confidence values and re-calculating metrics.

this provided a direct interpretation of the fraction of samples to provide an increase in scores. Both the BMA-100 and MCD-100 provided similar results (albeit, lower accuracy for BMA-100). The LLCM-100 resulted with near identical accuracies of the MCD-100 up to *ca.* 0.65 of samples remaining, where it plateaus (Fig. 5a). Interestingly, this corresponds to the same point in the uncertain efficiency plot where the maximum difference occurs for correct and incorrect model predictions

(Fig. 5b). We observed that both MCD-100 and LLCM-100 behaved near identical for the uncertain efficiency plot, while the BMA-100 resulted in a similar trend with slightly lower performance.

The results from the German Bank 2010 dataset and our LLCM provided comparable performances to BMA-100 and MCD-100; however, using only a single forward-pass of inputs as opposed to 100 sampling of network parameters. In fact, comparing the use of different hyperparameters resulted with near identical outcomes.

**Substrate (depth 2) dataset.** This datasets contains 5 classes of boulders, cobbles, rocks, pebbles/gravel, and sand/mud and is particularly challenging due class imbalance (*i.e.*, 75% sand/mud). In Table 6, the results for the non-ensemble (ResNet-CNN) and ensemble (BMA-100, MCD-100, and LLCM-100) networks are presented.

As was done for the German Bank 2010 dataset, we initially performed a deterministic ResNet-CNN model using class weighting and/or hyperparameters such as logit normalization and label smoothing (Table 6, ResNet-CNN). This resulted in modest performance for accuracy and calibration metrics. However, when using class weighting and label smoothing, performance dropped *ca.* 10% as compared to other configurations. In this case again, we observed that model calibration decreased when using logit normalization and label smoothing. The ensemble BMA-100 model performed comparably to the non-ensemble models (Table 6, BMA-100 vs. Non-ensemble); however, calibration metrics suggests that the model is poorly calibrated. We then performed MCD-100 as done previously where we obtained results comparable to non-ensemble models (Table 6, MCD-100 vs. Non-ensemble) and a similar set of calibration metrics. Our LLCM-100 results were near identical with respect to MCD-100 and comparable to BMA-100 (Table 6, LLCM vs. MCD-100 vs. BMA-100).

Reliability diagrams (Fig. 6) for the LLCM-100 non-calibrated and calibrated models using cross-entropy loss with (-/ + /-) or without (-/ - /-) logit normalization or label smoothing (-/ - /+) indicated the largest effect on calibration when using logit normalization (Fig. 6c). As seen with the German Bank 2010 dataset, that can be corrected by applying a re-calibration (Fig. 6d).

Overall, we observed less of an effect when viewing reliability diagrams of the Substrate (depth 2) dataset compared to the smaller German Bank 2010 dataset. It would be prudent to not only evaluate calibration metrics, but also to plot reliability diagrams to gain insight relating to under- and/or over-confidence. In fact, per-class reliability diagrams could be explored for additional details.

We next explored generating lists of uncertain samples for the three uncertainty evaluators, BMA-100, MCD-100 (-/ - /-), and LLCM-100 (-/ - /-). Here again, we varied a threshold of confidence values and calculated the accuracy and efficiency of the remaining samples. The resulting uncertain metric plots (Fig. 7) displayed similar trends as seen previously for the German Bank 2010 dataset (*vide supra*). The overall performance for all uncertainty evaluators were comparable

**Table 6:** Model performances using ensemble and non-ensemble models and the Substrate (depth 2) dataset.

Model <sup>1,2</sup>	Accuracy $\uparrow$	NLL $\downarrow$	BS $\downarrow$	ECE $\downarrow$
<b>Non-ensemble: ResNet-CNN (<math>p = 0.01</math>)</b>				
-/-/-	0.883	0.094 (0.107)	0.025 (0.029)	0.042 (0.031)
-/+/-	0.883	0.590 (0.114)	0.206 (0.035)	0.295 (0.039)
+/+/-	0.825	0.676 (0.179)	0.243 (0.057)	0.284 (0.047)
+/-/-	0.832	0.142 (0.162)	0.039 (0.044)	0.055 (0.040)
+/-/+	0.761	0.760 (0.459)	0.287 (0.151)	0.302 (0.234)
-/-/+	0.882	0.186 (0.100)	0.045 (0.025)	0.038 (0.036)
<b>Ensemble: BMA-100 (ResNet-BNN)</b>				
BNN	0.830	0.260	0.082	0.030
<b>Ensemble: MCD-100 (ResNet-CNN; <math>p = 0.01</math>)</b>				
-/-/-	0.885	0.100 (0.114)	0.027 (0.031)	0.034 (0.024)
-/+/-	0.884	0.624 (0.127)	0.221 (0.039)	0.318 (0.033)
+/+/-	0.827	0.723 (0.199)	0.264 (0.063)	0.312 (0.033)
+/-/-	0.836	0.153 (0.173)	0.042 (0.047)	0.043 (0.028)
+/-/+	0.773	0.768 (0.466)	0.291 (0.154)	0.309 (0.238)
-/-/+	0.886	0.191 (0.105)	0.046 (0.026)	0.044 (0.029)
<b>Ensemble: LLCM-100 (ResNet-LLCM; <math>M = 100</math>; <math>p = 0.01</math>)</b>				
-/-/-	0.879	0.106 (0.114)	0.029 (0.031)	0.038 (0.031)
-/+/-	0.879	0.741 (0.134)	0.281 (0.028)	0.382 (0.105)
+/+/-	0.814	0.528 (0.190)	0.180 (0.048)	0.203 (0.095)
+/-/-	0.822	0.158 (0.170)	0.043 (0.046)	0.053 (0.044)
+/-/+	0.776	0.761 (0.506)	0.289 (0.173)	0.345 (0.292)
-/-/+	0.879	0.187 (0.105)	0.045 (0.026)	0.041 (0.035)

<sup>1</sup> BMA: 100 models; MCD: 100 inference samplings; and LLCM: 100 committee members. <sup>2</sup> Models defined based on training hyperparameters using class weights / logit normalization / label smoothing (amount of smoothing, 0.1). These hyperparameters are either applied (denoted by +) or omitted (denoted by -). Values in parentheses are for calibrated models using calculated temperature(s) as previously described.

for both the uncertain accuracy and uncertain efficiency plots. The MCD-100 and LLCM-100 were near identical in regards to the uncertain metric plots, whereas the BMA-100 model was slightly less for the uncertain accuracy plot but essentially the same for the uncertain efficiency plot. Despite the Substrate (depth 2) dataset being heavily imbalanced, these uncertainty evaluators provided an approach to obtain uncertain samples.

In summary, our efforts for the German Bank 2010 and Substrate (depth 2) datasets was focused on establishing an efficient and accessible method to identify uncertain benthic images for review by subject matter experts. Our long-term goal is to incorporate an active learning framework where data pools of uncertain samples are created and a user-interface is provided for marine scientists to interact and re-evaluate uncertain samples. While the two commonly used approaches (*i.e.*, BMA and MCD) are options, they can be difficult to configure and require substantial compute time and hardware requirements. With millions of available benthic images, we require a simple and robust approach to provide prioritized lists of uncertain images. The LLCM option provides users with a simple and comparable approach, further simplifying existing strategies with reduced compute requirements and complex configurations.

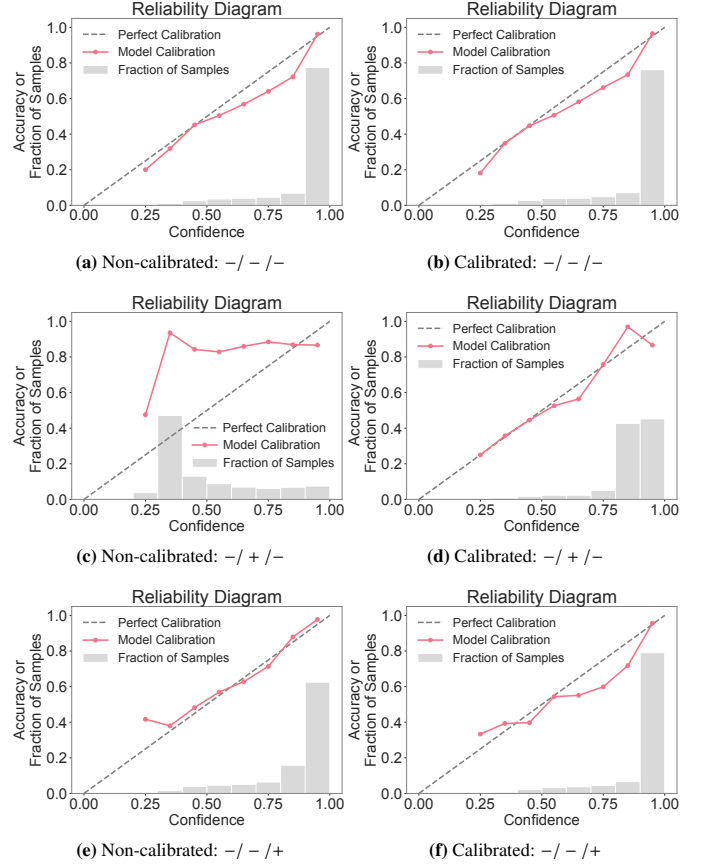


**Fig. 6:** Reliability diagrams for the Substrate (depth 2) dataset using a LLCM-100 network ( $p = 0.01$ ). Non-calibrated (left panels) and calibrated (right panels) using class weights / logit normalization / label smoothing (amount of smoothing, 0.1). These hyperparameters are either applied (denoted by +) or omitted (denoted by -).

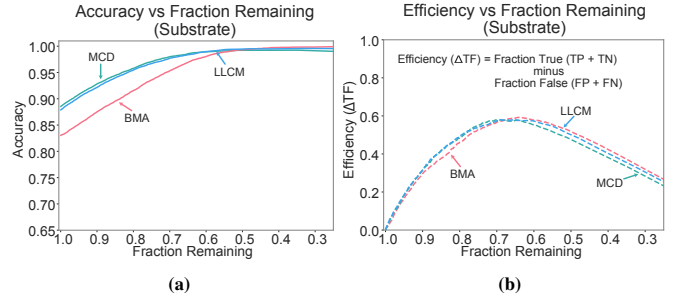


**Fig. 7:** Uncertain metric plots for the BMA-100, MCD-100 (-/-/-), and LLCM-100 (-/-/-) networks and the Substrate (depth 2) dataset using class weights / logit normalization / label smoothing (amount of smoothing, 0.1). These hyperparameters are either applied (denoted by +) or omitted (denoted by -). Each data point is created by applying increasing thresholds (step size 0.001) of confidence values and re-calculating metrics.

## 5. Conclusions

We compared our LLCM with commonly used Bayesian neural networks and Monte Carlo dropout inference samplings for the difficult benthic datasets, German Bank 2010 and Substrate (depth 2) using available pre-trained benthic models. We evaluated all networks using accuracy and uncertainty metrics such as NLL, BS, ECE, and in some cases, reliability dia-



grams. In addition, we investigated logit normalization and label smoothing as two approaches to mitigate over-confident predictions. These techniques appeared to degrade model calibration, which can be corrected using a temperature-scaling protocol, where optimal temperature(s) were determined using Bayesian optimization.

Our results shows that the LLCM is comparable to BMA and MCD methods. One particular advantage of the LLCM is that only a single forward-pass of inputs is required to obtain per-sample uncertainties. Whereas, both BMA and MCD require multiple inferences and then average output predictions to obtain per-sample uncertainties. Given the challenges of labeling benthic imagery, the size of the datasets, and the evolving nature of images in these datasets over time, LLCMs offers an efficient approach for Bayesian approximations. Prioritized lists of uncertain predictions can be generated and provided to marine scientists to re-evaluate and enhance existing approaches.

### CRedit authorship contribution statement

**H. Martin Gillis:** Conceptualization – Ideas; Methodology – Development or design of methodology; creation of models; Software; Writing – original draft; **Isaac Xu:** Writing – review & editing; **Benjamin Misiuk:** Writing – review & editing; **Craig J. Brown:** Writing – review & editing; **Thomas Trappenberg:** Supervision; Writing – review & editing.

### Declaration of competing interest

The authors declare that they have no known competing financial interests or personal relationships that could have appeared to influence the work reported in this paper.

### Data availability

The data and pre-trained models used for this study are publicly available from the following sources: BenthicNet: [Misiuk et al. \(2024\)](#); Lowe et al. (2025) & MNIST: [PyTorch \(2025a\)](#).

### References

Abdar, M., Pourpanah, F., Hussain, S., Rezazadegan, D., Liu, L., Ghavamzadeh, M., Fieguth, P., Cao, X., Khosravi, A., Acharya, U.R., Makarenkov, V., Nahavandi, S., 2021. A review of uncertainty quantification in deep learning: Techniques, applications and challenges. *Information Fusion* 76, 243–297. doi:[10.1016/j.inffus.2021.05.008](#).

Althaus, F., Hill, N., Edwards, L., Ferrari, R., 2014. CATAMI classification scheme for scoring marine biota and substrata in underwater imagery: A pictorial guide to the collaborative and annotation tools for analysis of marine imagery and video (CATAMI) classification scheme. Technical Report. CATAMI.org. doi:[https://catami.org/wp-content/uploads/sites/2/2023/03/CATAMI\\_Classification\\_Scheme\\_v1.4\\_Technical\\_document.pdf](#).

Althaus, F., Hill, N., Ferrari, R., Edwards, L., Przeslawski, R., Schönberg, C.H.L., Stuart-Smith, R., Barrett, N., Edgar, G., Colquhoun, J., Tran, M., Jordan, A., Rees, T., Gowlett-Holmes, K., 2015. A standardised vocabulary for identifying benthic biota and substrata from underwater imagery: The CATAMI classification scheme. *Public Library of Science ONE* 10, 1–18. doi:[10.1371/journal.pone.0141039](#).

Arbel, J., Pitas, K., Vladimirova, M., Fortuin, V., 2023. A primer on Bayesian neural networks: review and debates. arXiv preprint. doi:[10.48550/arXiv.2309.16314](#).

Arosio, R., Hobley, B., Wheeler, A.J., Sacchetti, F., Conti, L.A., Furey, T., Lim, A., 2023. Fully convolutional neural networks applied to large-scale marine morphology mapping. *Frontiers in Marine Science* 10. doi:[10.3389/fmars.2023.1228867](#).

Beijbom, O., Treibitz, T., Kline, D.I., Eyal, G., Khen, A., Neal, B., Loya, Y., Mitchell, B.G., Kriegman, D., 2016. Improving automated annotation of benthic survey images using wide-band fluorescence. *Scientific Reports* 6, 1–11. doi:[10.1038/srep23166](#).

Bingham, E., Chen, J.P., Jankowiak, M., Obermeyer, F., Pradhan, N., Karaletsos, T., Singh, R., Szerlip, P., Horsfall, P., Goodman, N.D., 2019. Pyro: deep universal probabilistic programming. *Journal of Machine Learning Research* 20, 973–978. URL: [https://jmlr.org/papers/volume20/18-403/18-403.pdf](#).

Brown, C.J., Sameoto, J.A., Smith, S.J., 2012. Multiple methods, maps, and management applications: Purpose made seafloor maps in support of ocean management. *Journal of Sea Research* 72, 1–13. doi:[10.1016/j.seares.2012.04.009](#).

Brown, C.J., Smith, S.J., Lawton, P., Anderson, J.T., 2011. Benthic habitat mapping: a review of progress towards improved understanding of the spatial ecology of the seafloor using acoustic techniques. *Estuarine, Coastal and Shelf Science* 92, 502–520. doi:[10.1016/j.ecss.2011.02.007](#).

Dosovitskiy, A., Beyer, L., Kolesnikov, A., Weissenborn, D., Zhai, X., Unterthiner, T., Dehghani, M., Minderer, M., Heigold, G., Gelly, S., Uszkoreit, J., Houlsby, N., 2021. An image is worth 16 × 16 words: transformers for image recognition at scale, in: *International Conference on Learning Representations (ICLR)*, pp. 1–22. doi:[10.48550/arXiv.2010.11929](#).

Egele, R., Maulik, R., Raghavan, K., Lusch, B., Guyon, I., Balaprakash, P., 2021. AutoDEUQ: automated deep ensemble with uncertainty quantification. arXiv preprint. doi:[10.48550/arXiv.2110.13511](#).

Gal, Y., Ghahramani, Z., 2015. Dropout as a Bayesian approximation: representing model uncertainty in deep learning, in: *International Conference on Machine Learning (ICML)*, pp. 1–12. doi:[10.48550/arXiv.1506.02142](#).

- Gal, Y., Hron, J., Kendall, A., 2017. Concrete dropout. arXiv preprint. doi:[10.48550/arXiv.1705.07832](https://doi.org/10.48550/arXiv.1705.07832).
- Gawlikowski, J., Tassi, C.R.N., Ali, M., Lee, J., Humt, M., Feng, J., Kruspe, A., Triebel, R., Jung, P., Roscher, R., Shahzad, M., Yang, W., Bamler, R., Zhu, X.X., 2023. A survey of uncertainty in deep neural networks. *Artificial Intelligence Review* 56, S1513–S1589. doi:[10.1007/s10462-023-10562-9](https://doi.org/10.1007/s10462-023-10562-9).
- Guo, C., Pleiss, G., Sun, Y., Weinberger, K.Q., 2017. On calibration of modern neural networks, in: *International Conference on Machine Learning (ICML)*, pp. 1–14. doi:[10.48550/arXiv.1706.04599](https://doi.org/10.48550/arXiv.1706.04599).
- Harrison, J., Willes, J., Snoek, J., 2024. Variational Bayesian last layers, in: *International Conference on Learning Representations (ICLR)*, pp. 1–33. doi:[10.48550/arXiv.2404.11599](https://doi.org/10.48550/arXiv.2404.11599).
- He, K., Zhang, X., Ren, S., Sun, J., 2016. Deep residual learning for image recognition, in: *Conference on Computer Vision and Pattern Recognition (CVPR)*, pp. 770–778. doi:[10.1109/CVPR.2016.90](https://doi.org/10.1109/CVPR.2016.90).
- Holm, A.N., Wright, D., Augenstein, I., 2023. Revisiting softmax for uncertainty approximation in text classification. *Information* 14. doi:[10.3390/info14070420](https://doi.org/10.3390/info14070420).
- Huang, G., Li, Y., Pleiss, G., Liu, Z., Hopcroft, J.E., Weinberger, K.Q., 2017. Snapshot ensembles: train 1, get M for free, in: *International Conference on Learning Representations (ICLR)*, pp. 1–14. doi:[10.48550/arXiv.1704.00109](https://doi.org/10.48550/arXiv.1704.00109).
- Huang, Z., Brooke, B.P., Harris, P.T., 2011. A new approach to mapping marine benthic habitats using physical environmental data. *Continental Shelf Research* 31, S4–S16. doi:[10.1016/j.csr.2010.03.012](https://doi.org/10.1016/j.csr.2010.03.012).
- Humboldt-Renaux, G., Johansen, A.S., Schmidt, J.E., Irilind, A.F., Madsen, N., Moeslund, T.B., Pedersen, M., 2024. Underwater uncertainty: a multi-annotator image dataset for benthic habitat classification, in: *European Conference on Computer Vision (ECCV)*, pp. 1–24. doi:[https://vbn.aau.dk/ws/portalfiles/portal/738329849/JAMB0-ECCV\\_vbn.pdf](https://vbn.aau.dk/ws/portalfiles/portal/738329849/JAMB0-ECCV_vbn.pdf).
- Hüllermeier, E., Waegeman, W., 2021. Aleatoric and epistemic uncertainty in machine learning: an introduction to concepts and methods, in: *Machine Learning*. Springer. volume 110, pp. 457–506. doi:[10.1038/s41597-025-04491-1](https://doi.org/10.1038/s41597-025-04491-1).
- Jackett, C., Althaus, F., Maguire, K., Farazi, M., Scoulding, B., Untiedt, C., Ryan, T., Shanks, P., Brodie, P., Williams, A., 2023. A benthic substrate classification method for seabed images using deep learning: Application to management of deep-sea coral reefs. *Journal of Applied Ecology* 60, 1254–1273. doi:[10.1111/1365-2664.14408](https://doi.org/10.1111/1365-2664.14408).
- Jospin, L.V., Buntine, W., Boussaid, F., Laga, H., Bennamoun, M., 2020. Hands-on Bayesian neural networks: A tutorial for deep learning users. doi:[10.1109/MCI.2022.3155327](https://doi.org/10.1109/MCI.2022.3155327).
- Katija, K., Orenstein, E., Schlining, B., Lundsten, L., Barnard, K., Sainz, G., Boulais, O., Cromwell, M., Butler, E., Woodward, B., Bell, K.L.C., 2022. Fathomnet: A global image database for enabling artificial intelligence in the ocean. *Scientific Reports* 12. doi:[10.1038/s41598-022-19939-2](https://doi.org/10.1038/s41598-022-19939-2).
- Lakshminarayanan, B., Pritzel, A., Blundell, C., 2017. Simple and scalable predictive uncertainty estimation using deep ensembles, in: *Conference on Neural Information Processing Systems (NeurIPS)*, pp. 1–15. doi:[10.48550/arXiv.1612.01474](https://doi.org/10.48550/arXiv.1612.01474).
- Lee, S., Purushwalkam, S., Cogswell, M., Crandall, D., Batra, D., 2015. Why M heads are better than one: training a diverse ensemble of deep networks. arXiv preprint. doi:[10.48550/arXiv.1511.06314](https://doi.org/10.48550/arXiv.1511.06314).
- Li, X., Wang, F. (Eds.), 2023. *Artificial intelligence oceanography*. Springer Nature Singapore. doi:[10.1007/978-981-19-6375-9](https://doi.org/10.1007/978-981-19-6375-9).
- Liu, P., Wang, L., Ranjan, R., He, G., Zhao, L., 2022. A survey on active deep learning: From model driven to data driven. *ACM Computing Surveys* 54, 1–34. doi:[10.1145/3510414](https://doi.org/10.1145/3510414).
- Louppe, G., Kumar, M., 2016. Bayesian optimization with *skopt*. URL: [https://scikit-optimize.github.io/stable/auto\\_examples/bayesian-optimization.html](https://scikit-optimize.github.io/stable/auto_examples/bayesian-optimization.html).
- Lowe, S.C., Misiuk, B., Xu, I., Abdulazizov, S., Baroi, A.R., Bastos, A.C., Best, M., Ferrini, V., Friedman, A., Hart, D., Hoegh-Guldberg, O., Ierodiaconou, D., Mackin-McLaughlin, J., Markey, K., Menandro, P.S., Monk, J., Neman, S., O'Brien, J., Oh, E., Reshitnyk, L.Y., Robert, K., Roelfsema, C.M., Sameoto, J.A., Schimel, A.C.G., Thomson, J.A., Wilson, B.R., Wong, M.C., Brown, C.J., Trappenberg, T., 2025. BenthicNet: A global compilation of seafloor images for deep learning applications. *Scientific Data* 12, 1–24. doi:[10.1038/s41597-025-04491-1](https://doi.org/10.1038/s41597-025-04491-1).
- Misiuk, B., Brown, C.J., 2024. Benthic habitat mapping: a review of three decades of mapping biological patterns on the seafloor. *Estuarine, Coastal and Shelf Science* 296, 1–27. doi:[10.1016/j.ecss.2023.108599](https://doi.org/10.1016/j.ecss.2023.108599).
- Misiuk, B., Lowe, S., Xu, I., 2024. BenthicNet. Federated Research Data Repository. doi:[10.20383/103.0614](https://doi.org/10.20383/103.0614).
- Neal, R.M., 1995. Bayesian learning for neural networks. Phd thesis. University of Toronto.
- Ovadia, Y., Fertig, E., Ren, J., Nado, Z., Sculley, D., Nowozin, S., Dillon, J.V., Lakshminarayanan, B., Snoek, J., 2019. Can you trust your model's uncertainty? evaluating predictive uncertainty under dataset shift, in: *Conference on Neural Information Processing Systems (NeurIPS)*, pp. 1–25. doi:[10.48550/arXiv.1906.02530](https://doi.org/10.48550/arXiv.1906.02530).

- Pearce, T., Leibfried, F., Brintrup, A., Zaki, M., Neely, A., 2018. Uncertainty in neural networks: Approximately bayesian ensembling, in: International Conference on Artificial Intelligence and Statistics (AISTATS), pp. 1–30. doi:[10.48550/arXiv.1810.05546](https://doi.org/10.48550/arXiv.1810.05546).
- PyTorch, 2025a. MNIST. URL: <https://pytorch.org/vision/main/generated/torchvision.datasets.MNIST.html>.
- PyTorch, 2025b. OneCycleLR. URL: [https://pytorch.org/docs/stable/generated/torch.optim.lr\\_scheduler.OneCycleLR.html](https://pytorch.org/docs/stable/generated/torch.optim.lr_scheduler.OneCycleLR.html).
- Raphael, A., Dubinsky, Z., Iluz, D., Benichou, J.I.C., Netanyahu, N.S., 2020. Deep neural network recognition of shallow water corals in the Gulf of Eilat (Aqaba). Scientific Reports 10, 1–11. doi:[10.1038/s41598-020-69201-w](https://doi.org/10.1038/s41598-020-69201-w).
- Simonyan, K., Zisserman, A., 2014. Very deep convolutional networks for large-scale image recognition, in: International Conference on Learning Representations (ICLR), pp. 1–14. doi:[10.48550/arXiv.1409.1556](https://doi.org/10.48550/arXiv.1409.1556).
- Smith, L.N., Topin, N., 2017. Super-convergence: Very fast training of neural networks using large learning rates. doi:[10.48550/arXiv.1708.07120](https://doi.org/10.48550/arXiv.1708.07120).
- Steger, S., Knoll, C., Klein, B., Fröning, H., Pernkopf, F., 2024. Function space diversity for uncertainty prediction via repulsive last-layer ensembles, in: Structured Probabilistic Inference & Generative Modeling workshop of ICML, pp. 1–16. doi:[10.48550/arXiv.2412.15758](https://doi.org/10.48550/arXiv.2412.15758).
- Szegedy, C., Vanhoucke, V., Ioffe, S., Shlens, J., Wojna, Z., 2015. Rethinking the Inception architecture for computer vision. arXiv preprint. doi:[10.48550/arXiv.1512.00567](https://doi.org/10.48550/arXiv.1512.00567).
- Valdenegro-Toro, M., 2023. Sub-ensembles for fast uncertainty estimation in neural networks, in: Proceedings of the International Conference on Computer Vision (ICCV) Workshops, pp. 4119–4127. doi:[https://openaccess.thecvf.com/content/ICCV2023W/LXCV/papers/Valdenegro-Toro\\_Sub-Ensembles\\_for\\_Fast\\_Uncertainty\\_Estimation\\_in\\_Neural\\_Networks\\_ICCVW\\_2023\\_paper.pdf](https://openaccess.thecvf.com/content/ICCV2023W/LXCV/papers/Valdenegro-Toro_Sub-Ensembles_for_Fast_Uncertainty_Estimation_in_Neural_Networks_ICCVW_2023_paper.pdf).
- Wei, H., Xie, R., Cheng, H., Feng, L., An, B., Li, Y., 2022. Mitigating neural network overconfidence with logit normalization. arXiv preprint. doi:[10.48550/arXiv.2205.09310](https://doi.org/10.48550/arXiv.2205.09310).
- Wen, Y., Tran, D., Ba, J., 2020. BatchEnsemble: an alternative approach to efficient ensemble and lifelong learning. arXiv preprint. doi:[10.48550/arXiv.2002.06715](https://doi.org/10.48550/arXiv.2002.06715).
- Winther, J.G., Dai, M., Rist, T., Hoel, A.H., Li, Y., Trice, A., Morrissey, K., Juinio-Meñez, M.A., Fernandes, L., Unger, S., Scarano, F.R., Halpin, P., Whitehouse, S., 2020. Integrated ocean management for a sustainable ocean economy. Nature Ecology and Evolution 4, 1451–1458. doi:[10.1038/s41559-020-1259-6](https://doi.org/10.1038/s41559-020-1259-6).
- Xie, J., Ma, Z., Lei, J., Zhang, G., Xue, J.H., Tan, Z.H., Guo, J., 2021. Advanced dropout: a model-free methodology for Bayesian dropout optimization. IEEE Transactions on Pattern Analysis and Machine Intelligence 44, 4605–4625. doi:[10.1109/TPAMI.2021.3083089](https://doi.org/10.1109/TPAMI.2021.3083089).
- Xu, I., Misiuk, B., Lowe, S.C., Gillis, H.M., Brown, C.J., Trappenberg, T., 2024. Hierarchical multi-label classification with missing information for benthic habitat imagery, in: International Joint Conference on Neural Networks (IJCNN), pp. 1–10. doi:[10.1109/IJCNN60899.2024.10650176](https://doi.org/10.1109/IJCNN60899.2024.10650176).
- Yasir, M., Rahman, A.U., Gohar, M., 2021. Habitat mapping using deep neural networks. Multimedia Systems 27, 679–690. doi:[10.1007/s00530-020-00695-0](https://doi.org/10.1007/s00530-020-00695-0).